Journal of Electroanalytical Chemistry 946 (2023) 117711

Contents lists available at ScienceDirect

Journal of Electroanalytical Chemistry

journal homepage: www.elsevier.com/locate/jelechem

Modeling of charging dynamics in electrochemical systems with a graphene electrode

Mahdi Yavarian [a,*], Roderick Melnik [b], Z.L. Mišković [a,c]

[a] Department of Applied Mathematics, University of Waterloo, Waterloo, ON, N2L 3G1, Canada
[b] MS2Discovery Interdisciplinary Research Institute, M2Net Lab, Wilfrid Laurier University, 75 University Avenue, Waterloo, ON N3L 3V6, Canada
[c] Waterloo Institute for Nanotechnology, University of Waterloo, Waterloo, ON, N2L 3G1, Canada

ARTICLE INFO

Keywords:
EIS
ECS
Graphene
Quantum capacitance
Knee frequency

ABSTRACT

A classical electrochemistry problem related to the polarization of a graphene electrode immersed in an aqueous solution and subjected to a small external ac voltage is revisited. The Poisson-Nernst-Planck equations with proper boundary conditions are linearized and normalized, leading to an analytical formula for the impedance of the electrochemical system containing a graphene-metal electrode pair. Electrochemical impedance spectroscopy is utilized to compare the impedance behavior of the graphene-metal electrode pair with the standard metal-metal electrode pair for a range of ion concentrations in the electrolyte. Also studied is the electrochemical capacitive spectroscopy to provide a detailed analysis related to the effects of the quantum capacitance of graphene on the total capacitive properties of the system.

1. Introduction

Electrochemical impedance spectroscopy (EIS), one of the several electrochemical methods available, has significantly increased the number of research, ranging from energy storage purposes to biological applications such as biosensors and immunosensors [1,2]. EIS is especially well adapted for evaluating various processes occurring at the electrode interface in response to the application of a low amplitude external difference of potential because it uses frequency-resolved measurements taken when the electrochemical system is in a steady-state. By varying the frequency of the applied perturbation, it is possible to separate the several timescales connected to the electrode-electrolyte interface, double-layer charging, electrochemical charge transfer, mass transport, and adsorption [1,2].

To develop strategies for increasing performance of an electrochemical cell, it is critical to understand the underlying mechanisms of the interfacial properties of the electrodes in contact with an electrolyte [3,4]. Besides the traditional electrodes such as metals, graphene-based electrodes have received much attention. Graphene has been found to be a promising electrode material for electric double-layer capacitors [5] because of its special electronic properties and, in particular, its quantum capacitance [3,5] which is distinct from Maxwell's electromagnetic geometric capacitance involving a dielectric sandwiched between highly conductive metallic electrodes [6]. Due to the low charge carrier density around the Dirac point [7], the quantum capacitance of a graphene electrode in an electrochemical cell predominates over its overall capacitance. On the other hand, for a homogeneous metal electrode, quantum capacitance is high because of the enormous electrical density of states at the Fermi level, contributing very little to the overall interfacial capacitance, which is therefore dominated by the Debye capacitance as confirmed by experimental measurements [5,8].

For direct impedance measurement, the majority of biological processes, such as antigen-antibody interactions, are unable to provide a signal with the required sensitivity. Two ways may be thought about to enhance the obtained signal. Applying an effective immobilization technique that allows for maximum loading of active antibodies or antigens is one option. The alternative strategy entails the alteration of the electrode using conductive materials to produce signal amplification. Among the various materials used to modify electrodes, carbon-based nanomaterials stand out as an appealing choice. As an electrode in electrochemical sensors, graphene has generated a lot of interest compared to other conventional metallic electrodes because of its huge surface-to-volume ratio, high mechanical strength, low cost, ease of manufacture, and high electrical and thermal conductivity [9,10]. In the ongoing search for label-free detection for a variety of proteins, the use of graphene as an electrode material has opened up a new field

* Corresponding author.
E-mail address: myavaria@uwaterloo.ca (M. Yavarian).

https://doi.org/10.1016/j.jelechem.2023.117711
Received 8 March 2023; Received in revised form 9 June 2023; Accepted 6 August 2023
Available online 10 August 2023

in electrochemistry with significantly improved performance and given researchers the chance to comprehend the very basic processes in the electrochemical capacitive interfaces [4,11].

Motivated by the above considerations, we propose an electrochemical cell containing a graphene-metal (GM) electrode pair. In the present work, we derive an analytic expression for the impedance of the cell in a neutral state equilibrium with appropriate boundary conditions when graphene is involved as an electrode. To reveal the role of graphene electrode, we purposefully idealized our model by assuming that the metal electrode has infinite (quantum) capacitance (ideal metal) [12,8,13–16] while neglecting the effects of heterogeneity and atomic steps [17]. Then, to highlight the significance of graphene electrode, in addition to EIS, we take advantage from analysis of the electrochemical capacitive spectroscopy (ECS) to compare the impedance behavior of GM electrode pair with that of the conventional metal-metal (MM) electrode pair.

The remaining portions of this paper are structured as follows: Section 2 outlines the theory of the concept, beginning with the linearization of the Poisson-Nernst-Planck (PNP) equations and the derivation of the appropriate boundary conditions. Having linearized the governing equations with taking advantage of a proper normalization, the impedance of the present electrochemical cell model is obtained. In Section 3, we discuss the impedance behavior of the present electrochemical system using the EIS, as well as the capacitive behavior through the ECS, highlighting the effects quantum capacitance of graphene. Finally, a conclusion with future directions is provided in Section 4.

2. Theory

In this part, we provide a straightforward model to explain how the ions in a symmetric 1:1 aqueous solution affect the impedance spectra. We begin by linearizing the PNP equations as governing equations, then derive a Robin type boundary condition assigned to graphene in the linear regime. Having linearized the equations and the boundary conditions, all the physical quantities are normalized to appropriate quantities in the Laplace domain. Finally, the normalized total impedance of the model is derived.

2.1. Linearized PNP equations

Fig. 1 illustrates a one-dimensional (in the x direction) electrochemical cell consisting of two planar, parallel, non-identical electrodes with large areas separated by an electrolyte layer of thickness of L. The cell is subjected to a time-dependent harmonic oscillating electric potential denoted by $V_a(t)$. The metal electrode is placed at $x = L$, while the electrode located at $x = 0$ is graphene. We derive a mathematical model for this structure using the following assumptions: (1) the electrolyte is binary containing only two ion species with opposite and equal valency, $z_+ = z_- = 1$, and with identical diffusion constants $D_+ = D_- = D$, along with equal mobilities $\mu_+ = \mu_- = \mu$ and identical bulk concentrations c_b in equilibrium, (2) the formation of a Stern layer (i.e., the contribution from the outer Helmholtz plane) at the surface of electrodes is ignored, (3) no adsorption/desorption processes take place for ions near either electrode, (4) both electrodes are blocking (non-Faradaic), hence, there is no charge transfer between the electrodes and the electrolyte (no Faradaic current) [18], and (5) the cell is in an overall neutral equilibrium state when it is perturbed by a small potential $V_a(t)$.

Considering these assumptions and using the Einstein's relation $\mu/D = e/k_BT$, the set of one-dimensional nonlinear PNP equations reads [19]

$$\frac{\partial C_\pm(x,t)}{\partial t} = -\frac{\partial}{\partial x}F_\pm(x,t), \tag{1}$$

$$F_\pm(x,t) = -D\left(\frac{\partial C_\pm(x,t)}{\partial x} \pm \frac{e}{k_BT}\frac{\partial \phi(x,t)}{\partial x}C_\pm(x,t)\right), \tag{2}$$

$$-\epsilon\frac{\partial^2\phi(x,t)}{\partial x^2} = e\left[C_+(x,t) - C_-(x,t)\right]. \tag{3}$$

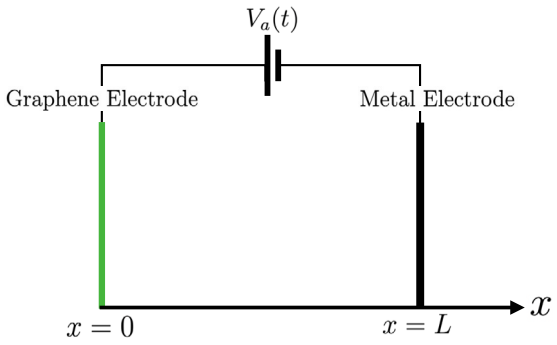

Fig. 1. One-dimensional schematic representation of the electrochemical cell containing graphene electrode in an aqueous solution. The time-dependent voltage $V_a(t)$ is applied to the electrolyte encapsulated between the GM electrode pair separated by L.

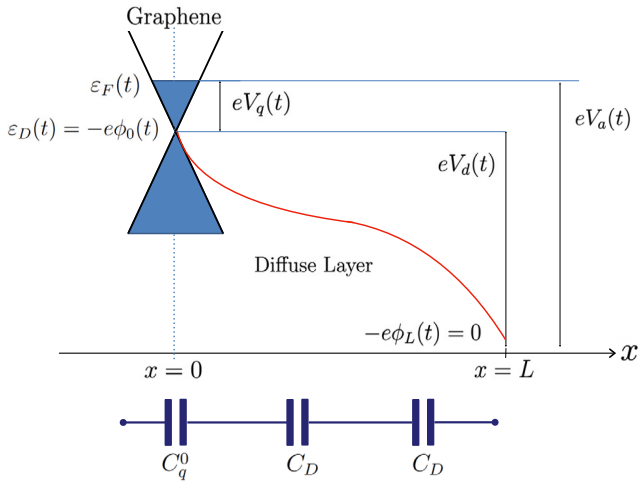

Fig. 2. Schematic diagram showing the electrostatic potential $\phi(x,t)$ as a function of distance x and electron energies with equivalent capacitors. The $\varepsilon_F(t)$ and $\varepsilon_D(t) = -e\phi(0,t) = -e\phi_0(t)$ are the time-dependent Fermi level and Dirac point assigned to graphene. Also shown are the potential differences that occur inside graphene at $x = 0$ giving rise to its doping, $V_q(t) = \phi_0(t) + \varepsilon_F(t)/e$, and the potential drop across the two diffuse layers, $V_d(t)$, that are adjacent to the graphene and metal electrodes. The C_q^0 at $x = 0$ is the quantum capacitance of graphene in equilibrium and C_D is the Debye capacitance [20].

Here, $C_\pm(x,t)$ refers to the concentrations of the positive and negative ions, $\phi(x,t)$ is the potential across the diffuse layer, $F_\pm(x,t)$ is the flux of the ions (Faradaic current), ϵ is the permittivity of the electrolyte, T is the temperature (300 K in this work), k_B is the Boltzmann constant, and $e > 0$ is the charge of a proton. Equation (1), taking into account Equation (2), describes the transport of the positive and negative ions, and Equation (3) is the equation of Poisson.

A schematic diagram associated with the doping of graphene via potential drop across the cell is shown in Fig. 2 along with equivalent capacitors [20]. In this figure, $\varepsilon_F(t)$ is the Fermi energy level of graphene at $x = 0$, $V_q(t)$ is the potential inside graphene linked to its doping, and $V_d(t)$ is the potential drop across the diffuse layer across the electrolyte region. The two cones represent low-energy portions of the π electron bands of graphene, which are treated in the so-called rigid band approximation [21] by positioning the Dirac point at the local value of the electric potential at the position of graphene, so that $\varepsilon_D(t) = -e\phi_0(t)$, where $\phi_0(t) \equiv \phi(0,t)$. Because the electrons in graphene respond to electric perturbations on a much shorter time scale than other time scales associated with ion motion in the electrolyte, we may assume that $\varepsilon_F(t)$, $\varepsilon_D(t)$ and $V_q(t) \equiv \left[\varepsilon_F(t) - \varepsilon_D(t)\right]/e$ follow instantaneously all the variations in the applied potential. Moreover, assuming that the potential at the metal electrode, $\phi_L(t) \equiv \phi(L,t)$, is zero, the po-

tential drop in the diffuse layer according to Fig. 2 is $V_d(t) = -\phi_0(t)$. Also shown are the equivalent capacitors for graphene as quantum capacitance in equilibrium represented by C_q^0 and two diffuse layers next to the electrodes, each represented by the Debye capacitance C_D (see below for the definition of those capacitances).

The introduction of a small AC perturbation to the applied voltage suggests that the quantities can be decomposed into an equilibrium part plus a small perturbed part denoted by δ throughout the present work. Assuming that the system is in a neutral state in equilibrium and neglecting the flat band effects (i.e., the constant potential offsets due to differences in the work function or in the electron affinity throughout the system), the terms corresponding to equilibrium parts of all the variables become zero, except for the ion concentrations that attain the value of the salt concentration in bulk region, denoted by c_b in this study. For the voltage variations much smaller than the thermal voltage, i.e., $\left|\delta V_{a,q,d}(t)\right| \ll k_B T/e$ along with applying the small signal approximation [22], the PNP equations can be linearized. Also, by defining $\delta C(x,t) = 1/2\left[\delta C_+(x,t) + \delta C_-(x,t)\right]$ and $\delta Q(x,t) = 1/2\left[\delta C_+(x,t) - \delta C_-(x,t)\right]$, as the mean ion concentration and the charge concentration, respectively, the linearized PNP equations can be expressed as

$$\frac{1}{D}\frac{\partial \delta C(x,t)}{\partial t} = \frac{\partial^2 \delta C(x,t)}{\partial x^2}, \tag{4}$$

$$\frac{1}{D}\frac{\partial \delta Q(x,t)}{\partial t} = \frac{\partial^2 \delta Q(x,t)}{\partial x^2} - \kappa^2 \delta Q(x,t), \tag{5}$$

$$-\epsilon \frac{\partial^2 \delta\phi(x,t)}{\partial x^2} = 2e\delta Q(x,t), \tag{6}$$

where $\kappa = \sqrt{2e^2 c_b/\epsilon k_B T}$ is the inverse Debye screening length [20]. In the above, Equation (4) shows that time evolution of the mean ion concentration is decoupled from the other two equations, Equation (5) is the Debye-Falkenhagen equation, and Equation (6) implies that the potential may be simply obtained by integrating the charge concentration $Q(x,t)$ twice with respect to x.

2.2. Boundary conditions

The linearized PNP system should be solved under the appropriate boundary conditions. The first set of boundary conditions comes from the fact the electrodes are blocking, meaning that there is no Faradaic current at the surface of the electrodes which yields $\delta F_{\pm}(0,t) = \delta F_{\pm}(L,t) = 0$. This gives the following boundary conditions for $\delta C(x,t)$ and $\delta Q(x,t)$ in the linearized PNP equations,

$$\left.\frac{\partial \delta C(x,t)}{\partial x}\right|_{x=0,L} = 0, \tag{7}$$

$$\left.\left[\frac{\partial \delta Q(x,t)}{\partial x} + \frac{ec_b}{k_B T}\frac{\partial \delta\phi(x,t)}{\partial x}\right]\right|_{x=0,L} = 0. \tag{8}$$

Note that, by considering Equation (4) and Equation (7), along with the initial condition $\delta C(x,0) = 0$, the solution to the diffusion equation Equation (4) is trivially obtained as $\delta C(x,t) = 0$, so this quantity is no longer needed in the following derivations.

Regarding the potential, we assume that the metal electrode is grounded, which gives another boundary condition as $\delta\phi(L,t) = 0$. In addition, applying the continuity of the potential and the Gauss's law at the surface of the graphene yields the potential at $x = 0^+$

$$\delta\phi(0,t) = -\delta V_d(t), \tag{9}$$

$$-\epsilon \left.\frac{\partial \delta\phi(x,t)}{\partial x}\right|_{x=0} = \delta\sigma_0(t), \tag{10}$$

in which $\delta\sigma_0(t)$ is the surface charge density of graphene. By linearizing $\delta\sigma_0(t)$ for small voltage fluctuation $\delta V_q(t)$ around the neutrality point, we may write approximately $\delta\sigma_0(t) = -C_q^0 \delta V_q(t)$, where C_q^0 is the quantum capacitance of a neutral, or intrinsic graphene, which is at finite temperature T evaluated as $C_q^0 = 4e^2 k_B T \ln 2/\pi\left(\hbar v_F\right)^2$ [23]. The derivation of the quantum capacitance of graphene away from neutrality point can be found in Appendix-A. Knowing that $\delta V_a(t) = \delta V_d(t) + \delta V_q(t)$, according to Fig. 2, we can eliminate $\delta V_d(t)$ and $\delta V_q(t)$ from Equation (9) and Equation (10), and obtain a Robin type inhomogeneous boundary condition for the potential at $x = 0^+$

$$\epsilon \left.\frac{\partial \delta\phi(x,t)}{\partial x}\right|_{x=0} - C_q^0 \delta\phi(0,t) = C_q^0 \delta V_a(t). \tag{11}$$

The above expression for the boundary condition pertaining to a graphene electrode is one of the main modeling results of this work.

2.3. Normalization and Laplace transform

Because the equations are linearized, we may now apply the Laplace transform, which replaces the dependence on time with a dependence on the new variable s that will be expressed in a steady-state regime of harmonic forcing at frequency ω as $s = i\omega$. Moreover, we introduce normalization for the independent variables according to $\bar{x} = \kappa x$, $\bar{L} = \kappa L$, $\bar{t} = t/\tau_D$, $\bar{s} = s\tau_D$ and $\bar{\omega} = \omega\tau_D$, with $\tau_D = 1/D\kappa^2$ being the Debye-Falkenhagen relaxation time [24]. Moreover, we normalize all the dependent variables, i.e., the perturbed quantities, according to $\overline{C} = \delta C/c_b$, $\overline{Q} = \delta Q/c_b$, $\overline{\phi} = e\delta\phi/(k_B T)$, whereas the perturbed electric current density will be normalized according to $\bar{J} = \delta J/J_{\lim}$, where $J_{\lim} = 2eDc_b\kappa$ is the limiting current [25]. Therefore, normalized system of Equation (5) and Equation (6) in the Laplace domain is written as

$$\bar{s}\,\overline{Q}(\bar{x},\bar{s}) = \overline{Q}''(\bar{x},\bar{s}) - \overline{Q}(\bar{x},\bar{s}), \tag{12}$$

$$\overline{\phi}''(\bar{x},\bar{s}) = -\overline{Q}(\bar{x},\bar{s}), \tag{13}$$

with corresponding boundary conditions

$$\overline{Q}'(\bar{x},\bar{s})\Big|_{\bar{x}=0,\bar{L}} + \overline{\phi}'(\bar{x},\bar{s})\Big|_{\bar{x}=0,\bar{L}} = 0, \tag{14}$$

$$\Gamma\overline{\phi}'(0,\bar{s}) - \overline{\phi}(0,\bar{s}) = \overline{V_a}(\bar{s}), \tag{15}$$

$$\overline{\phi}(\bar{L},\bar{s}) = 0, \tag{16}$$

in which we introduced the notation $\overline{Q}'(\bar{x},\bar{s}) = \partial\overline{Q}(\bar{x},\bar{s})/\partial\bar{x}$, $\overline{Q}''(\bar{x},\bar{s}) = \partial^2\overline{Q}(\bar{x},\bar{s})/\partial\bar{x}^2$, and similarly for $\overline{\phi}(\bar{x},\bar{s})$. In the graphene boundary condition, Equation (15), we defined a dimensionless parameter $\Gamma = C_D/C_q^0$ with C_D being the Debye capacitance defined as $C_D = \epsilon\kappa$. This parameter will play a key role in analyzing the effects of graphene in the overall impedance behavior of the cell in a broad range of equilibrium ion concentrations c_b.

2.4. Impedance of the electrochemical cell

To obtain the impedance of the cell, we need to determine the total current in the system. The total measurable current is independent of the position x [26] and it may be written as $\delta J(t) = \delta J_c(x,t) + \delta J_d(x,t)$, in which $\delta J_c(x,t) = e\left[\delta F_+(x,t) - \delta F_-(x,t)\right]$ is the conductive current and $\delta J_d(x,t) = -\epsilon\frac{\partial^2\delta\phi(x,t)}{\partial x\partial t}$ is the displacement current [27]. Knowing that the conductive current at the surface of the graphene is zero by the blocking electrode boundary condition, $\overline{J}_c(0,\bar{s}) = 0$, the total current in the cell may be calculated from the value of the displacement current at $x = 0^+$ as

$$\overline{J}(\bar{s}) = -\bar{s}\overline{\phi}'(0,\bar{s}). \tag{17}$$

The impedance of the electrochemical cell is defined as $\overline{Z}(\bar{s}) = \overline{U}(\bar{s})/\overline{J}(\bar{s})$ where $\overline{U}(\bar{s}) = -\overline{V}_a(\bar{s})$ is the applied potential to the graphene with respect to the grounded metal electrode (the current is flowing in the positive x direction) and $\overline{J}(\bar{s})$ is evaluated from the solutions of the system of equations obtained in Appendix-B. Therefore, the expression

for the impedance of the present electrochemical cell containing GM electrode pair is

$$\overline{Z}(\bar{s}) = \frac{\Gamma}{\bar{s}} + \frac{2}{\bar{s}(1+\bar{s})^{3/2}} \tanh\left(\sqrt{1+\bar{s}}\frac{\overline{L}}{2}\right) + \frac{\overline{L}}{1+\bar{s}}. \tag{18}$$

To explore the effects of a finite quantum capacitance of graphene, we can take advantage from the fact that the quantum capacitance of an ideal metal bulk electrode is often described as infinite [12,8,13–16]. This stems from an assumption that the electron density of states (DOS) in a metal electrode is so large that charging its surface with excess electrons or holes does not give rise to any appreciable shift of the Fermi energy level in the metal. In terms of the notation used in the diagram in Fig. 2, this would imply that $V_q(t) = 0$, which is of course inadequate for graphene with its low DOS near the Dirac point. However, to perform *formal* replacement of a graphene electrode by an ideal metal electrode at $x = 0$, it suffices to take the limit $C_q^0 \to \infty$, which renders $\delta V_q(t) = 0$ and reduces Equation (11) to $\delta\phi(0,t) = -\delta V_a(t)$ that replaces Equation (9), whereas the condition Equation (10) is no longer required because the charge on an ideal metal electrode is fully controlled by the potential drop across electrolyte. Therefore, the impedance of a cell containing two ideal metal electrodes is recovered by setting $\Gamma = 0$ in Equation (18) [28]. Note that, in that limit, the boundary condition Equation (15) becomes simply $\overline{\phi}(0,\bar{s}) = \overline{U}(\bar{s})$, as it should.

3. Results and discussion

The parameters applied in the calculations of this section are taken to represent an aqueous solution of the electrolyte at room temperature with $\epsilon = 80\,\epsilon_0$, where ϵ_0 is the vacuum permittivity, having the equilibrium ion concentration c_b corresponding to the neutral bulk region, which will be treated as a variable parameter of the system. We shall express c_b in moles per liter [29], expressed by M, which represents an aqueous solution of monovalent ions at room temperature with $\kappa \approx 3.236\sqrt{c_b}$ nm^{-1} and $C_D \approx 230\sqrt{c_b}$ μF/cm^2. With the graphene quantum capacitance at the room temperature being $C_q^0 \approx 0.8$ μF/cm^2, we can express $\Gamma \approx 287.5\sqrt{c_b}$. To be consistent with measured data used in [18,30], both impedance spectroscopy and capacitive spectroscopy in this study are evaluated for different bulk concentrations ranging from $c_b = 10^{-1}$ M to $c_b = 10^{-5}$ M with the normalized frequency $\bar{\omega}$ in the range of 0.001 – 1000. Also, the thickness of the electrolyte is taken to be $L = 1$ μm. Importantly, our discussion will be mainly focused on the low-frequency regime.

3.1. EIS analysis

Fig. 3 depicts the effects of ion concentration on the impedance behavior in the Nyquist plot. To capture the sole effects of ion concentration, the impedance is further normalized by the electrolyte thickness, $\hat{Z} = \overline{Z}/\overline{L} = \hat{Z}_r + i\hat{Z}_i$. Beginning from the origin as the high-frequency regime, it reveals that there is no offset near the origin of the Nyquist plot, indicating the absence of the ohmic resistance associated with the solution resistance, wires, clips, or other contacts [31,32] for both types of electrode pairs (GM and MM). The middle-frequency regime is represented by a semicircle for both types of electrode pair describing the effects of the electrolyte thickness and charging of the electrolyte layer. This region characterizes the movement of ions through the electrolyte layer (electrolyte polarization). Moving from the middle-frequency region to the low-frequency region, Fig. 3 shows an upward bending of the Nyquist curves with a smaller curvature. In this region, ions move across the double-layer region, and the charging process begins to develop, which may be viewed as the transition from diffusion to capacitance. The charging process is either controlled by the creation of the electric double layer (large slope) or is constrained by ion diffusion in the electrolyte depending on the slope of this region (small slope) [18]. According to the figure, the slope of the curves for both types of electrode pairs and all ion concentration values is vertical at small frequencies,

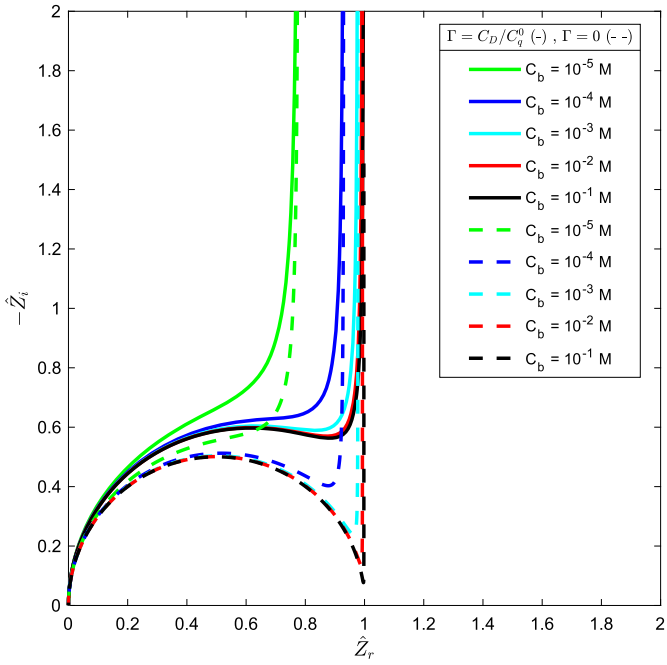

Fig. 3. Illustration of Nyquist Plot for different ion concentrations with the electrolyte thickness of L = 1 μm. The solid lines refer to the GM electrode pair, and the dashed lines refer to MM electrode pair.

suggesting that the charging process is largely determined by the region of the electric double layer in the absence of Faradaic reactions for both types of electrode pairs. This steep spike at low frequencies results from our assumption that both electrodes are blocking, or ideally polarized [32], so that only the displacement current (capacitive current) is allowed to participate at the surface of the electrodes.

Of particular interest in the Nyquist plot are the inflection points observed nearly at the tail of the middle-frequency regime in Fig. 3. Each inflection point may be identified as a knee frequency, accounting for how fast the charging–discharging process occurs. Therefore, the knee frequency can be considered a capacitor's capability for energy storage purposes [33,34]. To observe the behavior of the knee frequency with respect to variation of ion concentration, we numerically solved the equation $\hat{Z}_i''\hat{Z}_r' - \hat{Z}_i'\hat{Z}_r'' = 0$, in which the prime and double prime, respectively, denote the first and second derivatives with respect to the normalized frequency of $\overline{\omega}$. The solution to the above equation gives us the knee frequency, denoted by $\overline{\omega}_k$. Fig. 4 illustrates the numerical analysis of the knee frequencies as ion concentration changes for both types of electrode pairs. According to the figure, the knee frequencies of both electrode pairs tend to be linearly declined for low ion concentrations and are relatively comparable in this range of concentration (notice that the figure presents a log-log plot). As ion concentration increases, the knee frequencies of the MM electrode pair decrease linearly. However, the influence of ion concentration on knee frequencies for the GM electrode pair becomes weak, and little change is observed for concentrations exceeding $c_b \approx 10^{-3}$ M. Considering the trend of frequency in Fig. 4, we also notice that the knee frequency for the GM electrode pair is higher than that of the MM electrode pair for all ion concentrations, suggesting that a shorter time is needed to reach the capacitive behavior in the presence of a graphene electrode.

One of the drawbacks of the Nyquist plots is that the behavior of impedance is not quite obvious to frequency dispersion. To resolve this issue, the Bode phase plot and the Bode magnitude plot are often suggested and are therefore shown in Fig. 5 and Fig. 6, respectively. The Bode phase plot is defined as $\Phi = \arctan\left(\hat{Z}_i/\hat{Z}_r\right)$ with respect to frequency for different values of concentration and is expressed in degrees. As the frequency decreases, the phase for the GM electrode pair ap-

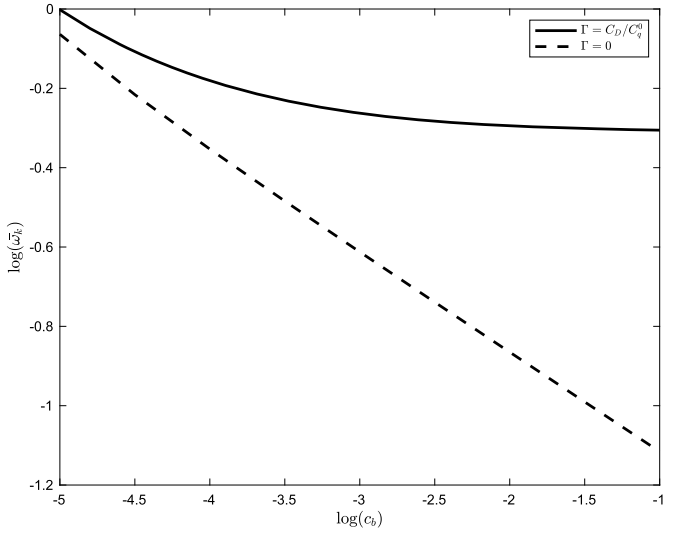

Fig. 4. The normalized knee frequency, $\overline{\omega}_k$ (defined in the text), is shown as a function of ion concentration c_b (expressed in the units of mole/liter) for the electrolyte thickness of L = 1 μm. The solid line refers to the GM electrode pair, and the dashed line refers to MM electrode pair.

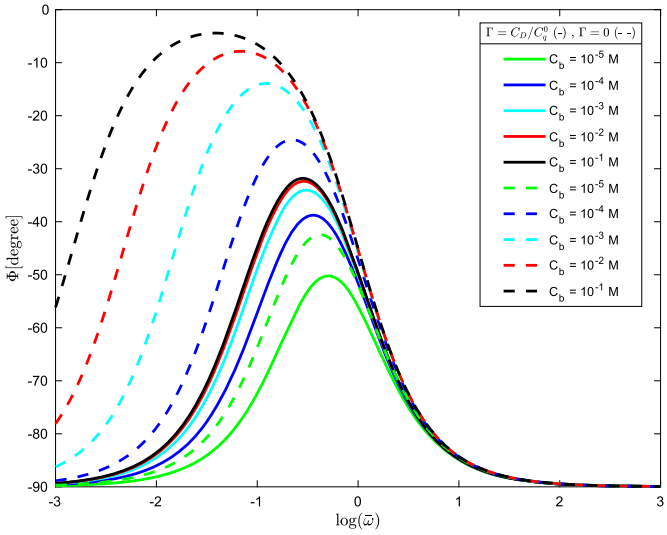

Fig. 5. Illustration of Bode phase plot for different concentrations with the electrolyte thickness of L = 1 μm. The solid lines refer to the GM electrode pair, and the dashed lines refer to MM electrode pair.

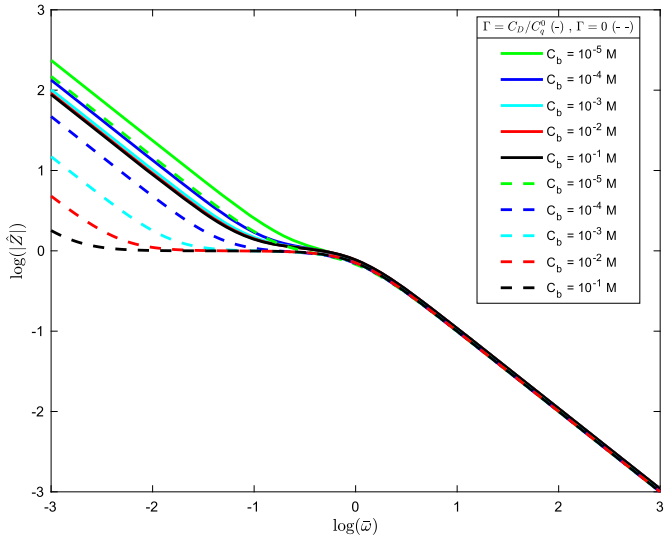

Fig. 6. Illustration of Bode magnitude Plot for different concentrations with the electrolyte thickness of L = 1 μm. The solid lines refer to the GM electrode pair, and the dashed lines refer to MM electrode pair.

proaches $\Phi = -90^0$ for all concentration values already at $\bar{\omega} \approx 10^{-3}$. For the MM electrode pair, such behavior only occurs at much lower frequencies than $\bar{\omega} = 10^{-3}$. As ion concentrations increase, the impedance characteristics of the MM electrode pair in the low-frequency regime tend to move away from capacitive behavior, almost reaching resistive behavior marked by $\Phi \approx 0$ for the highest concentration of $c_b = 10^{-1}$ M. Another highlighted impact of ion concentration is shifting the position of the peaks that appear in the plot, which can be attributed to sensitivity. According to the figure, the MM electrode pair shows a more prominent peak shift as ion concentrations increase than the GM pair. Therefore, in view of sensitivity, the MM electrode pair might be a promising candidate for choosing the frequency band that will provide the highest level of sensitivity for monitoring a biological target with a high ion content. Equally important is the angle of $\Phi = -45^0$ in which resistive and capacitive impedance become equal. Its corresponding frequency is known as the RC frequency because it signifies the change from being solely resistive (R) to being only capacitive (C), with the relaxation time scale being the minimal amount of time needed for a device with an efficiency of more than 50% to completely discharge all of its energy. [35–37]. An observation on the Fig. 5 reveals that, for the MM electrode pair, the RC frequency gradually shifts to the lower frequencies and, thus, higher time scales as the ion concentration increases. For the GM electrode pair, however, the RC frequency remains roughly the same for $c_b = 10^{-3}$ M, $c_b = 10^{-2}$ M, and $c_b = 10^{-1}$ M, and is obtained when $\overline{\omega} \approx 0.1$, leading to shorter time scale and higher efficiency.

A Bode plot of magnitude $|\hat{Z}| = \sqrt{\left(\hat{Z}_r\right)^2 + \left(\hat{Z}_i\right)^2}$ is shown in Fig. 6. The resistor only contains the real component and thus is frequency independent. In contrast, the capacitor will only have the imaginary component and be inversely proportional to frequency. As can be seen in Fig. 6, the impedance will consequently decrease with increasing frequency. Additionally, Bode magnitude charts with slopes close to −1 are typical of capacitive materials, whereas those with slopes close to 0 show resistive behavior [31]. Inspecting the figure at low frequencies reveals that the slope of the curves associated with the GM electrode pair for all ion concentrations tends to be −1, reflecting the fact that the impedance behavior is capacitive. However, the slopes of the curves for the MM electrode pair reach the value −1 at much lower frequencies, demonstrating a less capacitive and more resistive behavior compared to the GM electrode pair at intermediate frequencies. This result is also observed in the Bode phase plot. In the middle frequency regime, the curves become nearly flat with zero slope, exhibiting resistive behavior for both types of electrode pairs.

3.2. ECS analysis

Although EIS analysis provides important information concerning the electrochemical impedance behavior of the system, the emergence of quantum capacitance of graphene makes EIS analysis ineffective for data interpretations of the interfacial impedance when quantum effects are involved. This is because the Debye capacitance connected in series with the quantum capacitance of graphene brings about challenges in view of the capacitive distribution of the system when EIS is used. To resolve this issue, ECS is often used instead of EIS [38]. In the ECS analysis the complex impedance is converted into a complex capacitance via $\overline{C} = 1/\left(\overline{s}\overline{Z}\right) \equiv \overline{C}_r + i\overline{C}_i$ [39]. One sees that the very definition of complex capacitance magnifies the low-frequency behavior of the system, where the graphene electrode shows the most prominent effects. In terms of physical units, the normalized capacitance $\overline{C}$ and the complex

capacitance $C(s)$ are related as $\overline{C} = C(s)/C_D$. Although different plots of ECS may be suggested, in this study we only focus on the Nyquist capacitive plot.

Fig. 7 is the capacitive Nyquist plot of both types of electrode pairs for different values of concentration. As is shown in the figure, the Nyquist capacitive plot exhibits semicircles in which the intercepts of the $\overline{C}_r$ with horizontal axis give valuable information regarding the capacitive distribution at the low-frequency regime and high-frequency regime. In the low-frequency regime ($\bar{\omega} \ll 1$) with $\overline{L} \gg 1$, which is a valid approximation in majority of applications [40], the capacitance is evaluated as $\overline{C}_r(\overline{s}=0) = 1/(\Gamma+2)$. Recalling that $\Gamma = C_D/C_q^0$ and retrieving physical units, the capacitance in the low-frequency regime is found to be $C_r(\omega=0) = 1/\left(1/C_q^0 + 2/C_D\right)$, which gave rise to a graphical representation in terms of the equivalent circuit, shown in Fig. 2.

The low-frequency analysis can be made more transparent by performing a power expansion of the impedance, Equation (18), in terms of frequency $\bar{\omega}$ for finite $\overline{L}$. The first two leading terms in that power expansion yield an approximation for impedance in the form

$$\overline{Z} \approx \frac{1}{i\bar{\omega}\overline{C}_0} + \overline{R}_0, \tag{19}$$

where the first term gives a zero-frequency limit of the capacitance as

$$\overline{C}_0 = \left[\Gamma + 2\tanh\left(\frac{\overline{L}}{2}\right)\right]^{-1}, \tag{20}$$

whereas the second term gives a (suitably normalized) resistance in the zero-frequency limit as

$$\overline{R}_0 = \overline{L} + \frac{\overline{L}}{2}\operatorname{sech}^2\left(\frac{\overline{L}}{2}\right) - 3\tanh\left(\frac{\overline{L}}{2}\right). \tag{21}$$

On the other hand, for large frequencies, such that $\overline{L}\sqrt{\bar{\omega}} \gg 1$, we obtain an approximation for the impedance as

$$\bar{Z} \approx \frac{1}{i\bar{\omega}}(\Gamma + \overline{L}), \tag{22}$$

corresponding to an infinite-frequency limit of the capacitance $\overline{C}_r(\overline{s} \to i\infty) = 1/\left(\Gamma + \overline{L}\right)$, which gives in physical units $C_r(\omega \to \infty) = 1/\left(1/C_q^0 + 1/C_G\right)$, where $C_G = \epsilon/L$ is the geometric capacitance of the cell. Defining a graphene related length scale $\lambda_g^0 = \epsilon/C_q^0$, which takes the value $\lambda_g^0 \approx 89$ nm at room temperature, we may conclude that the high-frequency intercept of the capacitive Nyquist plot with the real axis is given by $C_r(\omega \to \infty) \approx C_G$ when the cell thickness is $L \gg \lambda_g^0$ for both types of electrode pairs, independent of the ion concentration. This is observed in Fig. 7 and its insert that emphasizes higher concentrations. Hence, we may conclude that the quantum capacitance of graphene should be most readily observable in measurements of the low-frequency intercept of the capacitive Nyquist plot with the real axis. This is especially true at low ion concentrations, when the inequality $C_q^0 \ll C_D$ should yield $C_r(\omega=0) \approx C_q^0 \approx 0.8\ \mu\text{F/cm}^2$.

4. Conclusions

In this study, we have derived an analytic expression for the impedance of an electrochemical cell containing graphene electrode. Beginning with linearization of the PNP equations and deriving the appropriate boundary conditions in the presence of graphene, the resulting system of equations is normalized and solved using the Laplace transform. A comparison of the impedance behavior of a GM electrode pair with that of a MM electrode pair was conducted over broad ranges of frequencies and ion concentrations. The EIS analysis has shown that GM electrode pair prevails over the MM electrode pair in exhibiting excellent capacitive behavior, shorter relaxation time scale, and high knee frequency. However, in terms of sensitivity to a variation in the ion concentration, we have seen that the MM electrode pair is more responsive

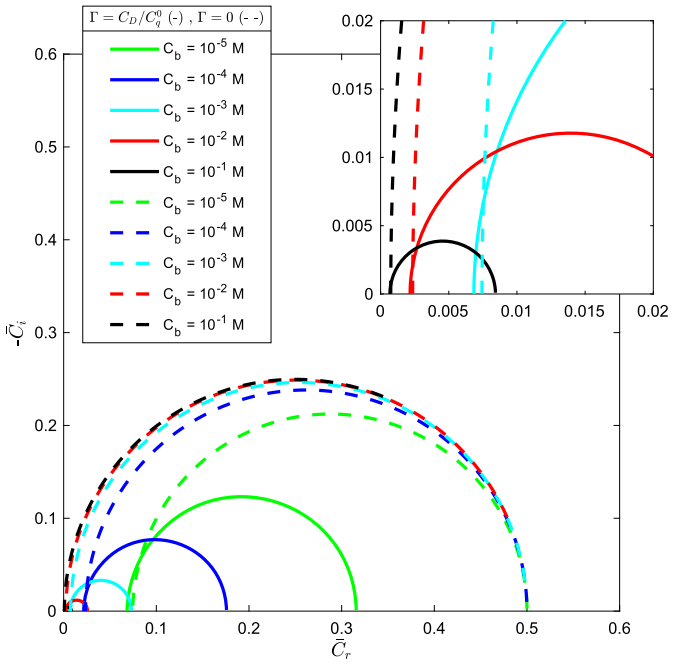

Fig. 7. Illustration of capacitive Nyquist Plot for different concentrations with the electrolyte thickness of L = 1 μm. The solid lines refer to the GM electrode pair, and the dashed lines refer to MM electrode pair. The inset magnifies the capacitive behavior at high-frequency regime.

compared to the GM electrode pair, especially at low frequencies and high ion concentrations.

In the ECS analysis, we have confirmed that the quantum capacitance of graphene may be reliably determined from the zero-frequency intercept with real axis in the Nyquist plot for equivalent capacitance of the cell, giving the total capacitance of the system, which is typically dominated by the quantum capacitance.

In future work, we shall make our calculations more realistic by including a contribution to the overall capacitance from the Stern layers, which can be readily done by solving Equation (12) and Equation (13) in piece-wise manner and implementing the standard electrostatic boundary/matching conditions at the outer Helmholtz planes near both electrodes [41]. This procedure gives rise to the so-called Stern boundary conditions on the electrodes, see Eq. (14) in Ref. [42]. It is interesting to notice that the graphene boundary condition in Equation (11) is isomorphic with the Stern boundary condition in Ref. [42], with their effective thickness of the Stern layer, λ_S, being replaced by the length scale due to graphene's interface with a medium of dielectric permittivity ϵ, defined by $\lambda_g = \epsilon/C_q$, which is bounded above by the value $\lambda_g^0 \approx 89$ nm for neutral graphene at room temperature that is independent of the equilibrium ion concentration. More importantly, we shall relax the assumption of a neutral equilibrium state for the electrochemical cell by generalizing the matched asymptotic analysis of Ref. [42] to the case of an asymmetric cell. In that case, a charged graphene electrode would still be described by a boundary condition of the type given in Equation (11), but with its quantum capacitance C_q determined by a constant value of the equilibrium doping potential, V_q^{eq}, via Equation (27) below.

CRediT authorship contribution statement

Mahdi Yavarian: Data curation, Formal analysis, Investigation, Methodology, Resources, Software, Validation, Writing – original draft, Writing – review & editing. **Roderick Melnik:** Funding acquisition, Project administration, Supervision. **Z.L. Mišković:** Conceptualization, Data curation, Formal analysis, Funding acquisition, Investigation,

Methodology, Project administration, Resources, Software, Supervision, Validation, Writing – review & editing.

Declaration of competing interest

The authors declare that they have no known competing financial interests or personal relationships that could have appeared to influence the work reported in this paper.

Acknowledgement

RM thanks the NSERC and the CRC Program for their support. ZLM acknowledges funding by NSERC (grant number 2023-03397).

Appendix A. Quantum capacitance of homogeneous monolayer graphene

The equilibrium number density of charge carriers in doped graphene is [20]

$$n(\mu_c) = \int_{-\infty}^{\infty} d\varepsilon \mathcal{D}(\varepsilon) \left[\frac{1}{1+\mathrm{e}^{\beta(\varepsilon-\mu_c)}} - \frac{1}{1+\mathrm{e}^{\beta\varepsilon}} \right] \tag{23}$$

where $\mu_c = eV_q(t)$ is the time-dependent chemical potential with respect to the state of undoped (neutral) graphene. For the sake of compactness, the dependency on time (t) is removed from the parameters in this appendix. Also, $\mathcal{D}(\varepsilon)$ is the density of states in graphene and $\beta = 1/k_BT$. For doping densities of interest in graphene applications, one typically has $|\mu_c| \lesssim 1$ eV, so it suffices to use linear approximation for the density of states $\mathcal{D}(\varepsilon) \approx 2|\varepsilon|/\left[\pi\left(\hbar v_F\right)^2\right]$, with $\varepsilon = 0$ corresponding to the Dirac point of graphene's π electron energy bands [20]. Knowing that the surface charge density of graphene is $\sigma_0 = -en(\mu_c)$, the quantum capacitance of graphene is evaluated as $C_q = -\frac{d\sigma_0}{dV_q} = e^2\frac{dn}{d\mu_c}$. We note that this may also be written as $C_q = \frac{k_{TF}}{2\pi}$, where k_{TF} is Thomas-Fermi inverse screening length due to polarization of the electron/hole system in doped graphene. Introducing $f\left(\varepsilon,\mu_c,\beta\right) = 1/\left(1+\mathrm{e}^{\beta(\varepsilon-\mu_c)}\right)$ as the Fermi-Dirac distribution and considering that $\partial f\left(\varepsilon,\mu_c,\beta\right)/\partial\mu_c = -\partial f\left(\varepsilon,\mu_c,\beta\right)/\partial\varepsilon$, the quantum capacitance of graphene is

$$C_q = e^2 \int_{-\infty}^{\infty} \mathcal{D}(\varepsilon)\left(-\frac{\partial}{\partial\varepsilon} f\left(\varepsilon,\mu_c,\beta\right)\right) d\varepsilon. \tag{24}$$

Performing the integration by parts gives

$$C_q = e^2 \int_{-\infty}^{\infty} f\left(\varepsilon,\mu_c,\beta\right)\left(\frac{d}{d\varepsilon}\mathcal{D}(\varepsilon)\right) d\varepsilon, \tag{25}$$

which yields

$$C_q = \frac{2e^2}{\pi\beta\left(\hbar v_F\right)^2}\left[\ln\left(1+e^{\beta\mu_c}\right) + \ln\left(1+e^{-\beta\mu_c}\right)\right]. \tag{26}$$

Retrieving $\beta = 1/k_BT$ and rearranging, the above equation can be expressed as

$$C_q = \frac{4e^2k_BT}{\pi\left(\hbar v_F\right)^2}\ln\left(2\cosh\left(\frac{eV_q}{2k_BT}\right)\right), \tag{27}$$

which is the quantum capacitance of a homogeneously-doped monolayer graphene. Note that by letting $V_q = 0$, the quantum capacitance of graphene at neutrality point is recovered as

$$C_q^0 = \frac{4e^2k_BT\ln 2}{\pi\left(\hbar v_F\right)^2}. \tag{28}$$

Appendix B. System of equations

With the definition of $p = \sqrt{1+\bar{s}}$, the Equ. (12) reduces to $\bar{Q}''(\bar{x},\bar{s}) - p(\bar{s})^2\bar{Q}(\bar{x},\bar{s}) = 0$ whose solution and its first derivative are readily found as

$$\begin{aligned} \bar{Q}(\bar{x},\bar{s}) &= A(\bar{s})e^{p(\bar{s})\bar{x}} + B(\bar{s})e^{-p(\bar{s})\bar{x}} \\ \bar{Q}'(\bar{x},\bar{s}) &= p(\bar{s})A(\bar{s})e^{p(\bar{s})\bar{x}} - p(\bar{s})B(\bar{s})e^{-p(\bar{s})\bar{x}} \end{aligned} \tag{29}$$

where $A(\bar{s})$ and $B(\bar{s})$ are integration constants. Using the above results, Equ. (13) leads to

$$\begin{aligned} \bar{\phi}'(\bar{x},\bar{s}) &= -\frac{A(\bar{s})}{p(\bar{s})}e^{p(\bar{s})\bar{x}} + \frac{B(\bar{s})}{p(\bar{s})}e^{-p(\bar{s})\bar{x}} + G(\bar{s}), \\ \bar{\phi}(\bar{x},\bar{s}) &= -\frac{A(\bar{s})}{p(\bar{s})^2}e^{p(\bar{s})\bar{x}} - \frac{B(\bar{s})}{p(\bar{s})^2}e^{-p(\bar{s})\bar{x}} + G(\bar{s})\bar{x} + H(\bar{s}), \end{aligned} \tag{30}$$

where $G(\bar{s})$ and $H(\bar{s})$ are two additional integration constants. Invoking the boundary conditions listed in Equs. (14) - (16) gives us the following system of equations

$$\begin{aligned} pA - \frac{A}{p} - \left(pB - \frac{B}{p}\right) + G &= 0 \\ \left(pA - \frac{A}{p}\right)e^{p\overline{L}} - \left(pB - \frac{B}{p}\right)e^{-p\overline{L}} + G &= 0 \\ \Gamma\left(-\frac{A}{p} + \frac{B}{p} + G\right) - \left(-\frac{A}{p^2} - \frac{B}{p^2} + H\right) &= \overline{V_a} \\ -\left(\frac{A}{p^2}\right)e^{p\overline{L}} - \left(\frac{B}{p^2}\right)e^{-p\overline{L}} + G\overline{L} + H &= 0 \end{aligned} \tag{31}$$

where the dependency of integration constants on ($\bar{s}$) is removed for the compactness of notation. The integration constants are obtained as

$$\begin{aligned} A &= -\frac{\overline{V_a}p^2}{\Delta} \\ B &= \frac{\overline{V_a}p^2e^{p\overline{L}}}{\Delta} \\ G &= \frac{\overline{V_a}p\left(p^2-1\right)\left(e^{p\overline{L}}+1\right)}{\Delta} \\ H &= -\frac{\overline{V_a}\left(e^{p\overline{L}} - p\overline{L} + p^3\overline{L} - \overline{L}pe^{p\overline{L}} + \overline{L}p^3e^{p\overline{L}} - 1\right)}{\Delta} \end{aligned} \tag{32}$$

where

$$\Delta = 2e^{p\overline{L}} - p\overline{L} + p^3\Gamma + p^3\overline{L} - p\overline{L}e^{p\overline{L}} + p^3\Gamma e^{p\overline{L}} + p^3\overline{L}e^{p\overline{L}} - 2 \tag{33}$$

References

[1] H.S. Magar, R.Y. Hassan, A. Mulchandani, Electrochemical impedance spectroscopy (eis): principles, construction, and biosensing applications, Sensors 21 (2021) 6578.
[2] V. Vivier, M.E. Orazem, Impedance analysis of electrochemical systems, Chem. Rev. 122 (2022) 11131–11168.
[3] A.J. Pak, E. Paek, G.S. Hwang, Impact of graphene edges on enhancing the performance of electrochemical double layer capacitors, J. Phys. Chem. C 118 (2014) 21770–21777.
[4] J.-H. Zhong, J.-Y. Liu, Q. Li, M.-G. Li, Z.-C. Zeng, S. Hu, D.-Y. Wu, W. Cai, B. Ren, Interfacial capacitance of graphene: correlated differential capacitance and in situ electrochemical Raman spectroscopy study, Electrochim. Acta 110 (2013) 754–761.
[5] C. Zhan, J. Neal, J. Wu, D.-e. Jiang, Quantum effects on the capacitance of graphene-based electrodes, J. Phys. Chem. C 119 (2015) 22297–22303.
[6] P.R. Bueno, J.J. Davis, Charge transport and energy storage at the molecular scale: from nanoelectronics to electrochemical sensing, Chem. Soc. Rev. 49 (2020) 7505–7515.
[7] S. Sun, Y. Qi, T.-Y. Zhang, Dissecting graphene capacitance in electrochemical cell, Electrochim. Acta 163 (2015) 296–302.
[8] P.A. Brooksby, A.K. Farquhar, H.M. Dykstra, M.R. Waterland, A.J. Downard, Quantum capacitance of aryldiazonium modified large area few-layer graphene electrodes, J. Phys. Chem. C 119 (2015) 25778–25785.
[9] Y. Shao, J. Wang, H. Wu, J. Liu, I.A. Aksay, Y. Lin, Graphene based electrochemical sensors and biosensors: a review, Electroanalysis 22 (2010) 1027–1036, An international journal devoted to fundamental and practical aspects of electroanalysis.

[10] L.J. Macedo, R.M. Iost, A. Hassan, K. Balasubramanian, F.N. Crespilho, Bioelectronics and interfaces using monolayer graphene, ChemElectroChem 6 (2019) 31–59.
[11] J. Cecchetto, A. Santos, A. Mondini, E.M. Cilli, P.R. Bueno, Serological point-of-care and label-free capacitive diagnosis of dengue virus infection, Biosens. Bioelectron. 151 (2020) 111972.
[12] C. Berthod, H. Zhang, A.F. Morpurgo, T. Giamarchi, Theory of cross quantum capacitance, Phys. Rev. Res. 3 (2021) 043036.
[13] B.C. Wood, T. Ogitsu, M. Otani, J. Biener, First-principles-inspired design strategies for graphene-based supercapacitor electrodes, J. Phys. Chem. C 118 (2014) 4–15.
[14] C. Zhan, C. Lian, Y. Zhang, M.W. Thompson, Y. Xie, J. Wu, P.R. Kent, P.T. Cummings, D.-e. Jiang, D.J. Wesolowski, Computational insights into materials and interfaces for capacitive energy storage, Adv. Sci. 4 (2017) 1700059.
[15] S.B. Desai, H.M. Fahad, T. Lundberg, G. Pitner, H. Kim, D. Chrzan, H.-S.P. Wong, A. Javey, Gate quantum capacitance effects in nanoscale transistors, Nano Lett. 19 (2019) 7130–7137.
[16] Q. Xu, G. Yang, W. Zheng, Dft calculation for stability and quantum capacitance of mos2 monolayer-based electrode materials, Mater. Today Commun. 22 (2020) 100772.
[17] M.B. Singh, R. Kant, Shape- and size-dependent electronic capacitance in nanostructured materials, Proc. R. Soc. A, Math. Phys. Eng. Sci. 469 (2013) 20130163.
[18] B.-A. Mei, O. Munteshari, J. Lau, B. Dunn, L. Pilon, Physical interpretations of Nyquist plots for edlc electrodes and devices, J. Phys. Chem. C 122 (2018) 194–206.
[19] A. Golovnev, S. Trimper, Exact solution of the Poisson–Nernst–Planck equations in the linear regime, J. Chem. Phys. 131 (2009) 114903.
[20] P. Sharma, Z.L. Mišković, Ionic screening of charged impurities in electrolytically gated graphene: a partially linearized Poisson-Boltzmann model, J. Chem. Phys. 143 (2015) 134118.
[21] A. Ochoa-Calle, A. Guevara-García, J. Vazquez-Arenas, I. González, M. Galván, Establishing the relationship between quantum capacitance and softness of n-doped graphene/electrolyte interfaces within the density functional theory grand canonical Kohn–Sham formalism, J. Phys. Chem. A 124 (2019) 573–581.
[22] R. Srinivasan, F. Fasmin, An Introduction to Electrochemical Impedance Spectroscopy, CRC Press, 2021.
[23] Z.L. Mišković, P. Sharma, F. Goodman, Ionic screening of charged impurities in electrolytically gated graphene, Phys. Rev. B 86 (2012) 115437.
[24] M.B. Singh, R. Kant, Debye–Falkenhagen dynamics of electric double layer in presence of electrode heterogeneities, J. Electroanal. Chem. 704 (2013) 197–207.
[25] J. Song, E. Khoo, M.Z. Bazant, Electrochemical impedance of electrodiffusion in charged medium under dc bias, Phys. Rev. E 100 (2019) 042204.
[26] A. Alexe-Ionescu, G. Barbero, L. Evangelista, E. Lenzi, Current–voltage characteristics and impedance spectroscopy: surface conduction and adsorption–desorption effects in electrolytic cells, J. Phys. Chem. C 124 (2020) 3150–3158.
[27] A. Alexe-Ionescu, G. Barbero, L. Evangelista, Electric response of asymmetric electrolytic cells to small ac signals, J. Electroanal. Chem. 873 (2020) 114378.
[28] G. Barbero, A. Alexe-Ionescu, Role of the diffuse layer of the ionic charge on the impedance spectroscopy of a cell of liquid, Liq. Cryst. 32 (2005) 943–949.
[29] J.N. Israelachvili, Intermolecular and Surface Forces, Academic Press, 2011.
[30] A. Koklu, V. Ajaev, A. Beskok, Self-similar response of electrode polarization for binary electrolytes in parallel plate capacitor systems, Anal. Chem. 91 (2019) 11231–11239.
[31] A.R. Bredar, A.L. Chown, A.R. Burton, B.H. Farnum, Electrochemical impedance spectroscopy of metal oxide electrodes for energy applications, ACS Appl. Energy Mater. 3 (2020) 66–98.
[32] P.M. Monk, Fundamentals of Electroanalytical Chemistry, John Wiley & Sons, 2008.
[33] S.A. Balogun, O.E. Fayemi, Effects of electrolytes on the electrochemical impedance properties of nipcmwcnts-modified glassy carbon electrode, Nanomaterials 12 (2022) 1876.
[34] M. Arunkumar, A. Paul, Importance of electrode preparation methodologies in supercapacitor applications, ACS Omega 2 (2017) 8039.
[35] N.O. Laschuk, E.B. Easton, O.V. Zenkina, Reducing the resistance for the use of electrochemical impedance spectroscopy analysis in materials chemistry, RSC Adv. 11 (2021) 27925–27936.
[36] J. Song, M.Z. Bazant, Electrochemical impedance of a battery electrode with anisotropic active particles, Electrochim. Acta 131 (2014) 214–227.
[37] W.-W. Liu, Y.-Q. Feng, X.-B. Yan, J.-T. Chen, Q.-J. Xue, Superior micro-supercapacitors based on graphene quantum dots, Adv. Funct. Mater. 23 (2013) 4111–4122.
[38] F.A. Gutierrez, F.C.B. Fernandes, G.A. Rivas, P.R. Bueno, Mesoscopic behaviour of multi-layered graphene: the meaning of supercapacitance revisited, Phys. Chem. Chem. Phys. 19 (2017) 6792–6806.
[39] L.C. Lopes, A. Santos, P.R. Bueno, Measuring quantum conductance and capacitance of graphene using impedance-derived capacitance spectroscopy, Carbon 184 (2021) 821–827.
[40] J.R. Macdonald, E. Barsoukov, Impedance Spectroscopy: Theory, Experiment, and Applications, John Wiley & Sons, 2018.
[41] L. Daniels, M. Scott, Z. Mišković, The role of Stern layer in the interplay of dielectric saturation and ion steric effects for the capacitance of graphene in aqueous electrolytes, J. Chem. Phys. 146 (2017) 094101.
[42] M.Z. Bazant, K. Thornton, A. Ajdari, Diffuse-charge dynamics in electrochemical systems, Phys. Rev. E 70 (2004) 021506.